

1. Output fluctuation of RE

Factors ruling mutual smoothing effect

Renewable energy (RE) output deviates naturally. To mitigate impacts caused by the output fluctuation, additional investment becomes necessary in power system side. By the way, total output of RE with geographical diversity is reduced by “mutual smoothing effect”. If the effect can be quantitatively grasped and can be incorporated into impact assessment, surplus additional investment can be avoided. Past researches only qualitatively studied the effect but could not incorporate it into impact assessment qualitatively. The difficulty is solved in the chapter.

These four factors rule mutual smoothing effect in importance order.

- 1) Fluctuation speed. Fast fluctuation is well smoothed out.
- 2) Area size. Fluctuation is well smoothed out in large area.
- 3) Number of RE. Fluctuation of many REs is well smoothed out
- 4) Uneven distribution. Fluctuation is well smoothed out in even distribution.

To totally handle various speed fluctuations, it is useful to transform fluctuation on time axis into that on frequency axis, that is, spectrum. For the purpose Fast Fourier Transform (FFT) is prepared as an useful tool.

1/10 decade method⁽¹⁾

However, there is a difficulty in FFT. Fig. 1.1 is fluctuation spectrum of a 275kW wind turbine processed by FFT from one month time sequential data. Spectrum is expressed as longitudinal line without thickness. Since the figure is painted out by the expression, only tops are plotted. Usually some smoothing process is applied to FFT results. Past researches do not show what type of smoothing is applied, and therefore, physical meaning of smoothed out data is not clear.

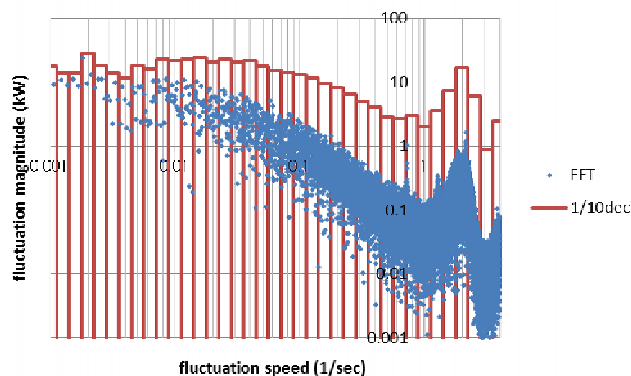


Fig. 1.1 Spectrum of a medium sized wind turbine

The author employs 1/10 decade method, which divides one decade fluctuation speed range into equal ten bands in logarithm axis and makes Pythagoras sum of fluctuation elements within a band as height of the band. 1/10 decade spectrum is expressed columns as shown in the figure. In 1/10 decade expression, $1/f$ fluctuation that is often seen in natural fluctuation is becomes flat. In the figure fluctuation slower than 0.1/sec is flat. Faster fluctuation is reduced by -1 powered speed. The tendency is very often seen in natural phenomena. The cause is inertia of blade in this case. A peak at very fast speed means tower shadow effect. By these merit 1/10 decade method is employed in acoustic field, and standards are established in IEC and JIS, and measurement equipment named “spectrum analyzer” is sold in market, but 1/10 decade method is not referred in texts. Since the expression by columns is laborious, a simplified expression by folded line linking centers of column head is employed hereafter.

Fig. 1.2 is 15 sites’ spectra during March to May, 2010. At 24 hour and 12 hour swing period found two peaks, which are always seen in irradiance spectra. Difference in the 15 sites’ spectra is very little, and as the result,

average spectrum is not much different from each site's spectrum. The figure shows $\Sigma(\Delta P)/N$, which is average of swing magnitude of every 1/10 decade band, and phase of element is ignored. Therefore, mutual smoothing effect does not appear. To incorporate mutual smoothing effect, time sequential average irradiance of the 15 sites is transformed by FFT and processed by 1/10 decade method, and spectrum $\Delta(\Sigma P)/N$ is calculated. The result is shown in Fig. 1.3. $\Delta(\Sigma P)/N$ that incorporate mutual smoothing effect is much smaller than $\Sigma(\Delta P)/N$ that does not incorporate mutual smoothing effect at 10 hour swing period or faster fluctuation.

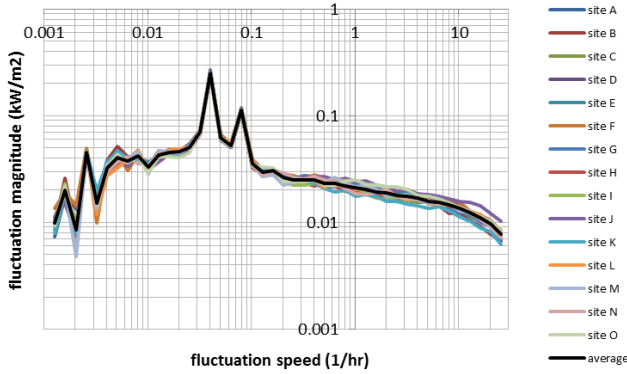


Fig. 1.2 Spectra of 15 sites' irradiance

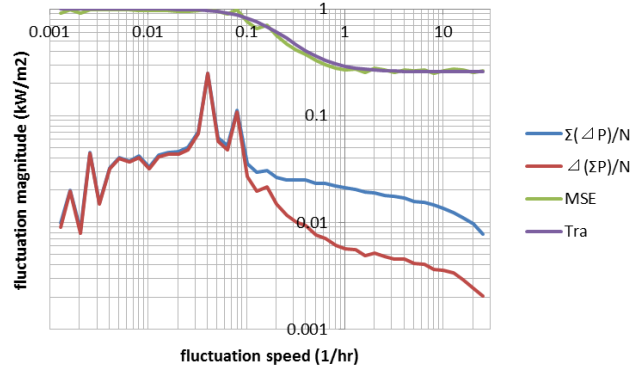


Fig. 1.3 Spectrum of 15 sites' average spectrum

Transfer Hypothesis⁽²⁾

In past researches mutual smoothing effect (MSE) is not clearly defined. The author defines it as follows. By the definition MSE value takes 0 to 1 value.

$$\text{MSE} = \frac{\Delta(\Sigma P)/N}{\Sigma(\Delta P)/N} \quad (1.1)$$

Character of RE output fluctuation is known as Table 1.1. Slow fluctuation is coherent (Coherent theory). Fast fluctuation

is random (Random theory) and $1/\sqrt{N}$ theory is available. The author presents "Transfer hypothesis" shown in equation (1.2) for mathematical express of these characters of MSE. Here, f is fluctuation speed, N is number of REs. T_x is a characteristic value of the area named "transfer swing period". Transfer hypothesis shows that mutual smoothing effect does not work in slow fluctuation, gradually becomes to work as fluctuation becomes faster than T_x , and fully works at sufficiently fast fluctuation and $1/\sqrt{N}$ theory becomes available. Absolute in right side, because MSE is achieved geographically and instantly, and therefore no time delay or phase delay is included.

$$\text{Tra}(N) = \left| \frac{1 + j T_x f / \sqrt{N}}{1 + j T_x f} \right| \quad (1.2)$$

Mutual smoothing effect (MSE) and transfer hypothesis (Tra) are also shown in Fig. 1.3. Transfer hypothesis is a good approximation of MSE. Error becomes minimum by setting T_x as 7.2 hour. High peaks at 24 and 12 hour swing period are seen in $\Delta(\Sigma P)/N$ and $\Sigma(\Delta P)/N$, but are not seen in MSE and transfer hypothesis. Because, MSE is made by dividing $\Delta(\Sigma P)/N$ by $\Sigma(\Delta P)/N$ as equation (1.1), and transfer hypothesis is approximation of MSE.

Factors ruling transfer swing period⁽³⁾

Transfer swing period T_X does not change by RE number N . It is thus demonstrated. Slower fluctuation than T_X is supposed to be coherent in two sites P and Q with distance D as shown in Fig. 1.4, and the coherency is lost in faster fluctuation. A third point R appears within the area covered by two circles with radius D whose centers are P and Q . Here, R is nearer to P than Q . Since distance RP is shorter than D , slower fluctuations than T_X of R and P is coherent. In faster fluctuations than T_X coherency of P , Q , and R is lost because coherency of P and Q is already lost. Thus, T_X does not change if a new site R joins. (Q. E. D.)

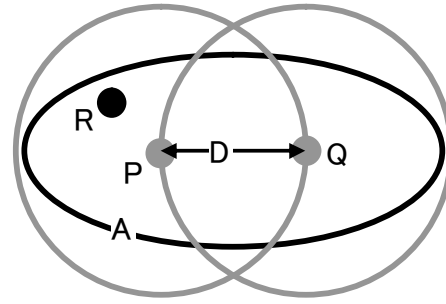


Fig. 1.4 Reason why T_X does not change

Here supposed an elips A just covered the two circles. Shorter distance of additional site in A to P or Q is always shorter than D . Therefore, T_X does not change. Thus it is found that T_X of area A is equal to T_X of two sites apart $1/3$ of major axis of area A .

Relationship between distance D of two sites and transfer swing period T_X is shown in Fig. 1.5. Irradiance data of Hokuriku 15 sites and that of 17 sites in a distribution line. (Their measuring time is different.)

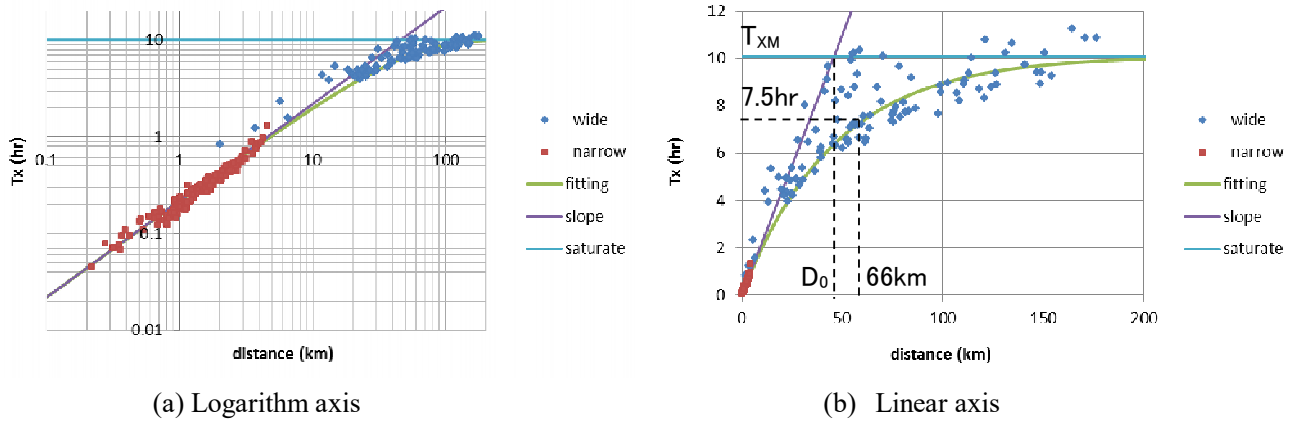


Fig. 1.5 Relationship between distance D of two sites and T_X

The relationship can be expressed equation as follows.

$$T_X = T_{XM} \{1 - \exp(-D / D_0)\} \quad (\text{hr}) \quad (1.3)$$

The equation can be approximated as “ $T_X \cong T_{XM} D / D_0$ ” in small D region, as “ $T_X \cong T_{XM}$ ” in large D region. Minimizing error, saturated value T_{XM} is identified as 10.1hr, D_0 as 46km. Major axis of Hokuriku region is 198km from east end (east end of Toyama pref.) to west end (Tsuruga city). $1/3$ of that is 66km, and corresponding T_X is 7.5 hour yhat is identified by equation (1.2). Using the theory, T_X can be found without long-term irradiance measurement in many sites.

Seasonal variation of transfer swing period T_X ⁽³⁾

According to the theory in the former section, T_X only depends on area size but does not depend on seasonal factors. Since definition of MSE in equation (1.1) includes division, error becomes large when denominator and numerator are small. Role of MSE becomes fatal in scenes with large RE fluctuation. Therefore, T_X can be regarded

as constant by time if variation of T_X is little in large RE fluctuation seasons.

Relationship between power spectra faster than 10 hour swing period σ_{10h}^2 and T_X is calculated from irradiance data of Hokuriku 20 sites during January to December of 2011. The results are shown in Fig. 1.6 by month and in Fig. 1.7 by week. Since peaks in irradiance spectra are seen at 24 and 12 hour swing period, but is not seen at 8 hour swing period, 10 hour swing period or faster can be regarded as fast PV fluctuation. T_X of months and weeks with large RE fluctuation scatter in narrow band: 7 to 8 hour. Therefore, seasonal T_X variation can be neglected.

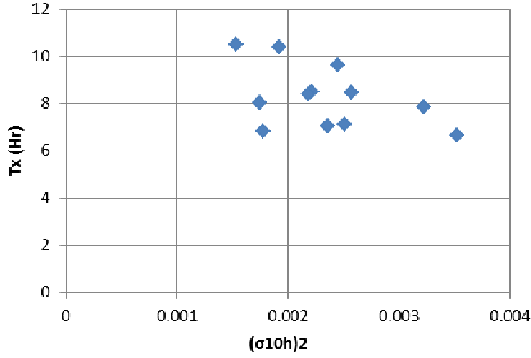


Fig. 1.6 T_X variation by month

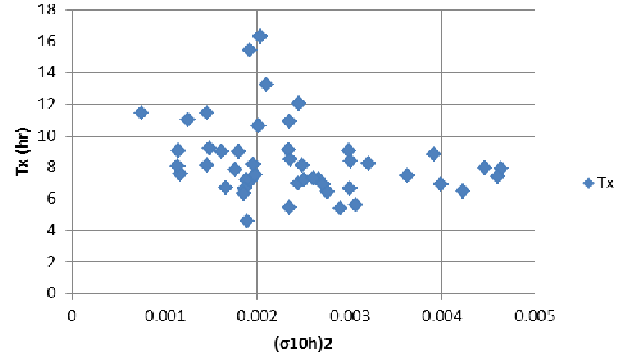


Fig. 1.7 T_X variation by week

Total fluctuation of highly penetrated RE⁽²⁾

When RE fluctuation of single site is ΔP , total fluctuation of N sites ΔP_N can be expressed as follows by eq. (1.2)

$$\Delta P_N = N \Delta P \text{Tra}(N)$$

Amplification factor when RE increase N sites to M sites considering MSE: $\Delta P_M / \Delta P_N$ can be expressed as follows.

$$\frac{\Delta P_M}{\Delta P_N} = \frac{M \Delta P \text{Tra}(M)}{N \Delta P \text{Tra}(N)} = \frac{M}{N} \left| \frac{1 + j T_X f / \sqrt{M}}{1 + j T_X f / \sqrt{N}} \right| \quad (1.4)$$

When PV that generate 4kW under 1KW/m² irradiance locates at every Hokuriku 15 irradiance measurement sites, total output considering MSE is $4 \times 15 \text{Tra}(15)$. 1540MW output PVs penetrate in Hokuriku, which corresponds 53GW in Japan, and each PV size is 4kW, number of PVs is $1540/0.004 = 385000$. Therefore, amplification factor from 15 sites can be calculated as follows.

$$\frac{385000}{15} \left| \frac{1 + j T_X f / \sqrt{385000}}{1 + j T_X f / \sqrt{15}} \right|$$

Spectrum of the case is obtained as Fig. 1.8. Since V does not generate in night, PV spectrum in a long time corresponds $1/\pi$ of fluctuation at noon. Therefore, $1/\pi$ of demand fluctuation is drawn as reference in the figure. Faster PV fluctuation than 1 hour period does not exceed demand fluctuation.

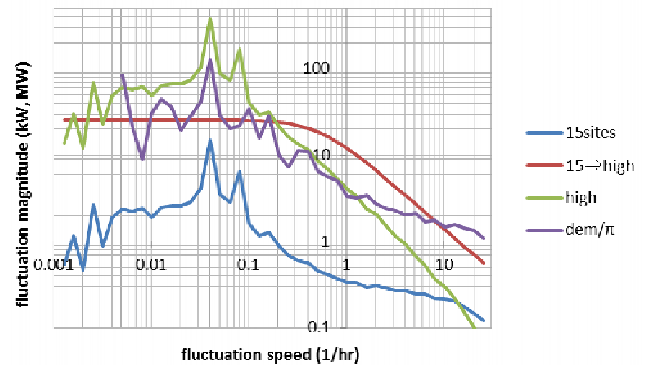


Fig. 1.8 Spectrum of highly penetrated PVs

Uneven distribution of RE⁽⁴⁾

A regulated core and space structure as Fig. 1.9 is supposed. REs distributed only in cores densely. MSE of the structure becomes as Fig. 1.10. T_x does not change because area size does not change (A). Swing speed at which fluctuation just comes to random (B) depend on distance of neighboring sites. As the result, fast fluctuation becomes larger than even distribution case. Here, N is number of REs, D is distance of neighboring REs in even distribution case, N_c is number of cores, D_c is distance of neighboring REs in uneven distribution case. Of course, N_c is much smaller than N , D_c is much shorter than D .

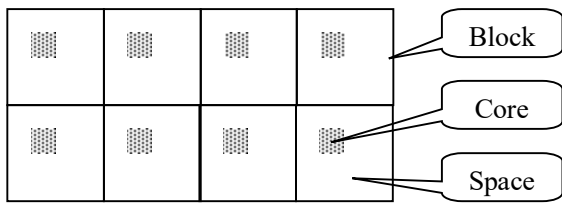


Fig. 1.9 Core and space structure

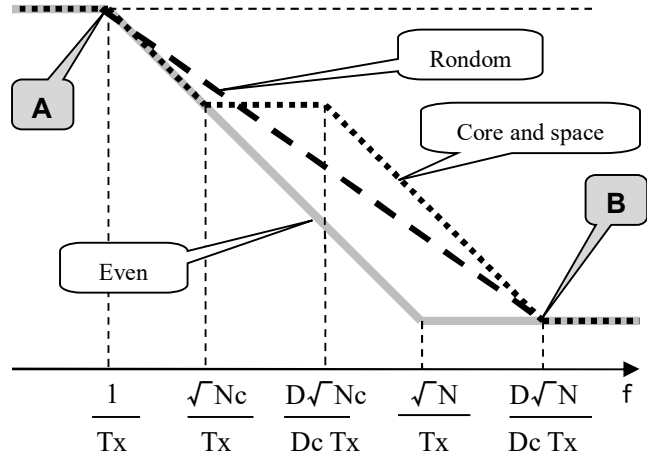


Fig. 1.10 MSE of RE uneven distribution

MSE of the case is expressed as follows. Left half of right side means inter-block MSE and right half does intra-block MSE.

$$Tra(N_c, N) = \begin{vmatrix} 1 + j \frac{T_x f}{\sqrt{N_c}} & 1 + j \frac{D_c T_x f}{D\sqrt{N}} \\ 1 + j T_x f & 1 + j \frac{D_c T_x f}{D\sqrt{N_c}} \end{vmatrix} \quad (1.5)$$

Number of 4kW REs penetrated 1540MW into 4300km² Hokuriku region is calculated as follows.

$$N = 1540000\text{kW} / 4\text{kW} = 385000$$

Supposing block size is 10km², number of cores is calculated as follows.

$$N_c = 4300\text{km}^2 / 10\text{km}^2 = 430 \text{ cores}$$

Distance of neighboring REs in even distribution case is calculated as follows.

$$D = \sqrt{4300\text{km}^2 / 385000} = 0.105683 \text{ km}$$

Distance of neighboring REs in cores is assumed as follows supposing densely built residences.

$$D_c = 0.02 \text{ km}$$

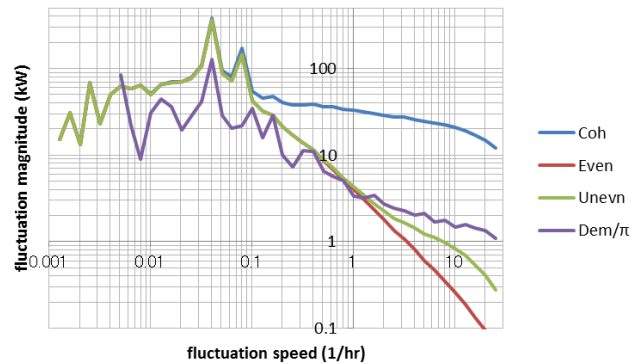


Fig. 1.11 Spectrum of core and space structured PV

PV is assumed as RE. In core and space structure case, spectrum is calculated as Fig. 1.11. Since long-term PV spectrum becomes $1/\pi$ of fluctuation at noon, $1/\pi$ of demand fluctuation is shown as reference in the figure. Fast fluctuation as several minutes of uneven case is 3 times larger than even case, but does not exceed demand fluctuation.

However observing real distribution of residences, orderly core and space structure is not seen, but REs distribute random. In these cases, concrete clues are only A and B points in the figure. If so, bald line on A and B will not differ from reality. The bald line is expressed as follows.

$$\text{Tra}(M) = \left| \frac{1 + j \left(\frac{D_c T_x f}{D\sqrt{M}} \right)^K}{1 + j (T_x f)^K} \right| \quad (1.6)$$

Spectrum core and space structured PV There is an unknown parameter K, which must be identified. Here focusing that very fast fluctuation magnitude must be same of result from eq. (1.6), parameter K must fulfill the condition as follows.

$$\left(\frac{D_c}{D\sqrt{N}} \right)^K = \frac{1}{\sqrt{N}}$$

Therefore, parameter K is identified as follows.

$$K = \frac{\log \frac{1}{\sqrt{N}}}{\log \frac{D_c}{D\sqrt{N}}} \quad (1.7)$$

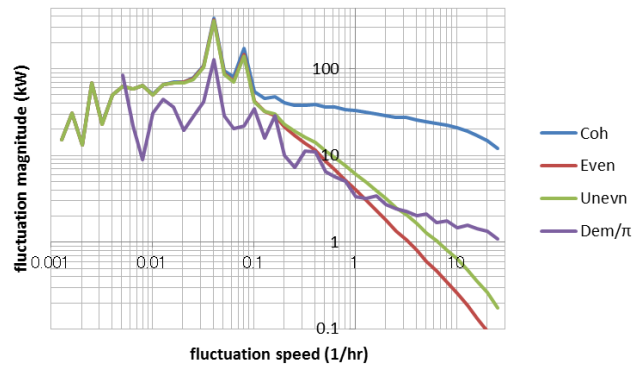


Fig. 1.12 Spectrum of random structured PV

1/10 decade spectrum when 1540MW PVs penetrate in Hokuriku region in the random uneven distribution is calculated as Fig. 1.12. Like former cases, $1/\pi$ of demand fluctuation is shown. RE fluctuation of random distribution is 2 times larger than even distribution case in a wide speed range from several hours period to several minutes period. Also, speed range where RE output fluctuation does not exceed demand fluctuation is restricted at in minutes period or faster speed range.

Applying MSE to time sequential data⁽²⁾

Approximate expression of MSE is expressed as eq. (1.2), which is a kind of low pass filter without phase delay, can also be applied to time sequential data. A series of methodology is shown in Fig. 1.13. Time sequential data of N sites: P(N) are transformed into spectrum: S(N) by FFT, and 1/10 decade processing is not employed. Applying reverse FFT to S(N), original time sequential data P(N). Thus, P(N) on time axis and S(N) on frequency axis are equivalent. Applying transfer hypothesis on S(N), spectrum S(M) of increased sites. Applying reverse FFT to S(M), time sequential presumed data P(M).

As an example, presumed time sequential variation on highly penetrated PV output in Fig. 1.14. Time sequential variation that is amplified the 15 site's average irradiance $K \cdot P(15)$ contains considerable fast fluctuation. However, presumed variation that considered adequate MSE is considerably smoothed out.

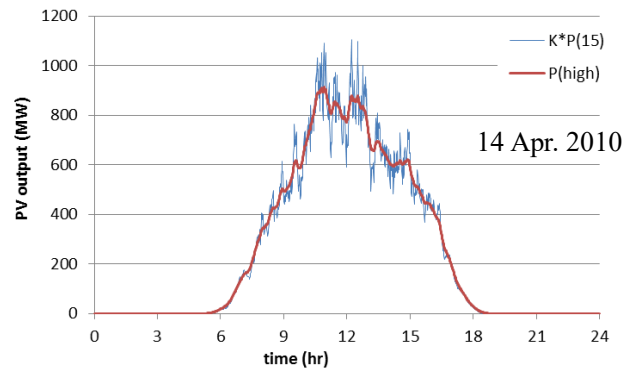
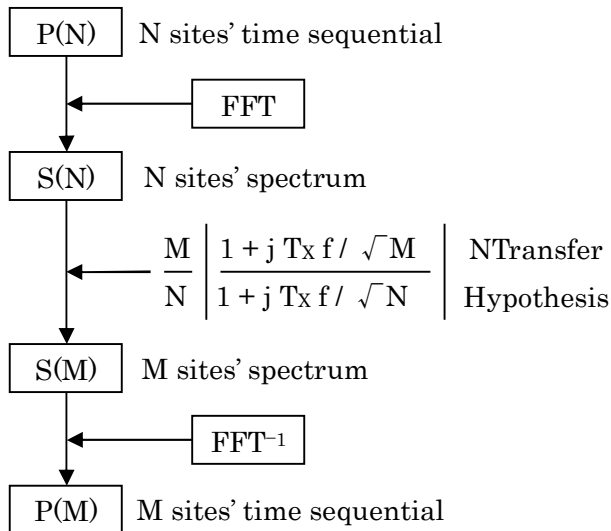


Fig. 1.14 Time sequential output of highly penetrated PVs

Fig. 1.13 Applying transfer hypothesis to time sequential data

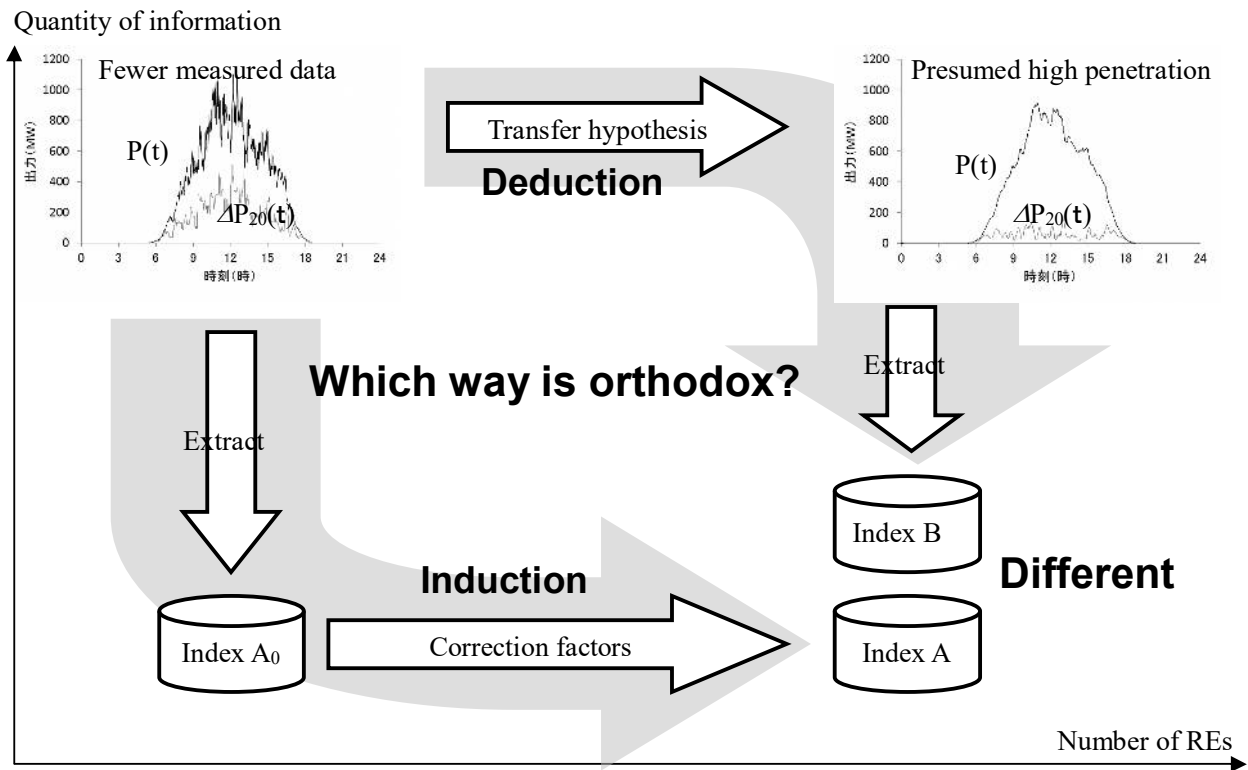


Fig. 1.15 Difference between traditional methods and transfer hypothesis

Since transfer hypothesis can be applied to time sequential data, is superior to the other theories. For evaluating battery LFC the merit is indispensable. In Fig. 1.15 traditional method and transfer hypothesis is compared focusing on information quantity⁽⁵⁾. Traditional method much reduces information quantity at the beginning by extracting index such as “maximum fluctuation in 20 minutes window”. Since much information is abandoned at the beginning, adequate presumption of total index when RE highly penetrates is impossible even though every countermeasure is taken. On the contrary transfer hypothesis presumes highly penetrated RE output fluctuation without reducing information quantity, therefore, is more reliable than traditional methods.

Translation of irradiance to output

Thus irradiance is presumed. However for practical use, irradiance must be translated to output. Occupational scientists propose sampling investigation of existing REs. For reliable parameter identification around 2000 data are needed. Time and cost are also needed. The author, practicing engineer, proposes to identify the translation factor based on measured irradiance and monthly sell/buy record from REs that utilities have. The idea uses already existing records, therefore, time and cost is quite reduced. Some utilities agree to the author’s method. On the contrary, sampling investigation of existing REs does not begin.

Battery LFC⁽⁶⁾

It is quite probable that some batteries are introduced for frequency regulation. Battery is more useful as regulation device than as mere negative reserve. Possible operational output range of existing thermal generation is shown in Fig. 1.16. To serve $\pm 5\%$ LFC capability, 40% output in average is needed. If battery serve LFC, some thermal generation can operate at minimum output or stop, and reduced 20 to 40% output can be used as negative reserve.

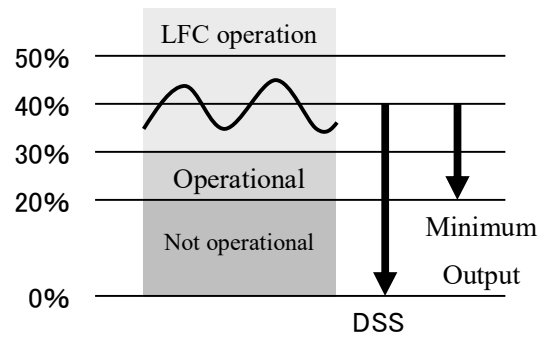


Fig. 1.16 Output range of thermal generation

Since battery LFC is high speed, LFC burden lean more to battery than to conventional generator. Battery should absorb residual error if possible so that conventional generator do not reduce their LFC burden. If not, additional amount of battery is needed because of silly control technique. For the purpose control as Fig. 1.17 is introduced. The control gives conventional generators sum of tie line flow P_{TIE} and battery output P_{BAT} as reference signal. As the result, conventional generators operate as if battery does not exist. To battery tie line flow is given as reference signal.

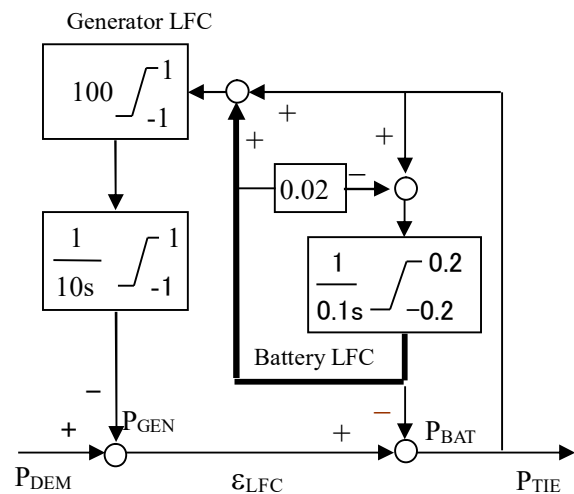


Fig. 1.17 Complementally control of battery and generator

To verify effect of the proposed battery LFC, a simple simulation is performed. Continuous triangle wave is given as demand variation (Dem). The results are shown in Fig. 1.18. Generator output (P_{gen}) under conventional LFC does not change by introduction of battery LFC. Tie line flow w/o battery almost turns to battery output (Batt), and tie line flow fluctuation ‘Tie) is kept very small. Also, effect of conventional LFC and battery LFC can be distinguished.

Is battery LFC useful in existing power system? To answer the question, a simple simulation is performed. LFC controlled generators are represented by one machine. Existing LFC controlled generators can vary their output at least 4%/minute of their rate output, which is inherited also by the represented machine. For simplicity, outer power system is far larger, and LFC can be modeled as FTC (Flat Tie-line Control). Residual error is larger when time lag of control loop is larger. 0.5 minute time lag can reproduce residual error of existing power system.

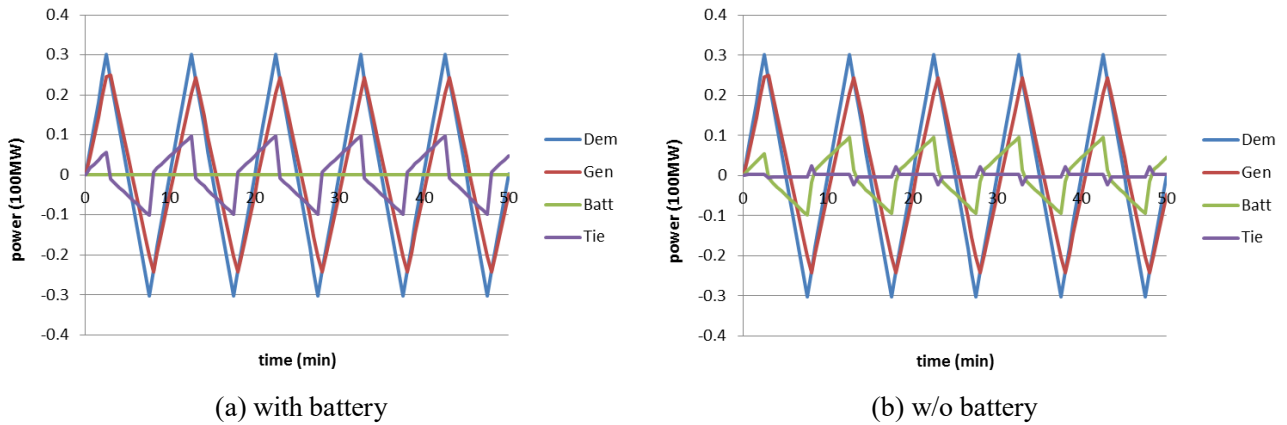


Fig. 1.18 Effect of battery LFC

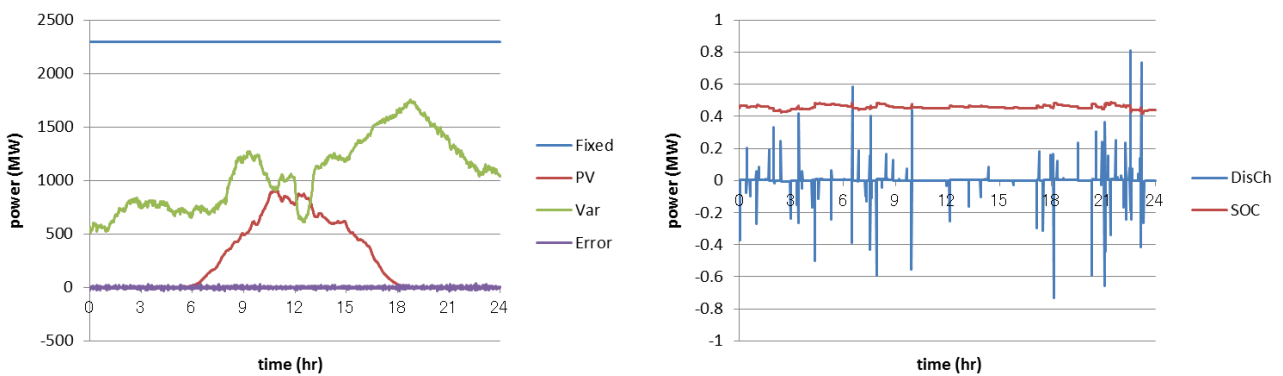


Fig. 1.20 Battery LFC with high PV penetration (Demand: 14 April 2010)

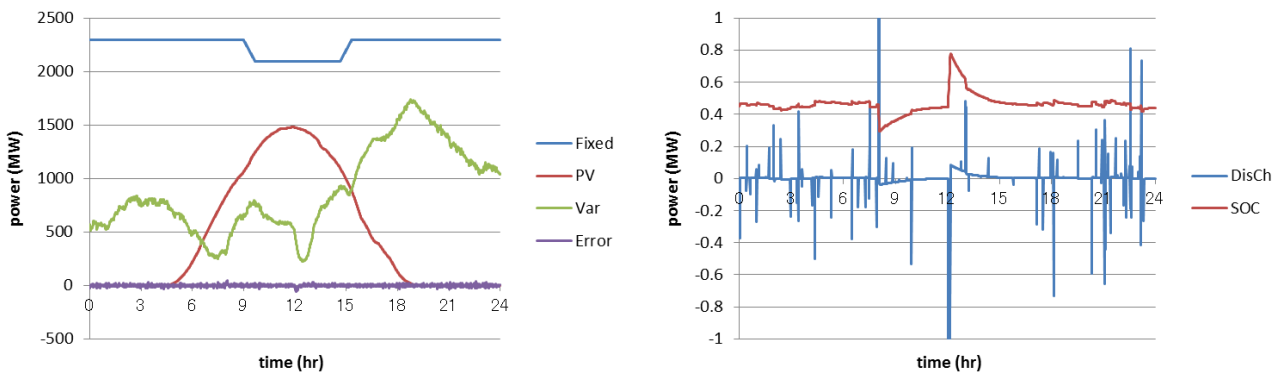


Fig. 1.21 Battery LFC with high PV penetration (Demand: 15 May 2010)

Presumed battery LFC performance in 14 April 2010 is shown in Fig. 1.20. Irradiance varied very much. LFC controlled generator have some margin to minimum LFC operational output. Large residual error does not appear. Battery can reduce residual error by complementing slow output change of LFC generator. But this is over quality. Battery’s charge/discharge does not reach rated power.

Presumed battery LFC performance in 15 May 2010 is shown in Fig. 1.21. Irradiance was high during daytime. Bottom of LFC controlled generator is reduced to 210MW because one machine stopped due to demand supply balance. Preparing demand dip at noon output of fixed output generator is reduced by 200MW, but output of LFC controlled generator is reduced to 224MW, which is near bottom. Residual error becomes large and charge and discharge power reaches to rated power.

Battery LFC is more useful in high irradiance day than in high irradiance variation day.

Ramp variation of RE⁽¹⁾

Aspect of wind power is somewhat different from PV. Slow and large ramp variation caused by such as passing front is regarded more serious than periodical variation. Definition of ramp variation is not established. Here, definition of Fig. 1.22, that is, difference of two average values of $T_w/2$ time windows apart T_w is adopted. By shifting the two windows minute by minute, data are stored. The definition has two merit. One is variation speed $\Delta P / T_w$ is preserved in constant speed variation. Another is reduction of data number is negligible small, and the merit gives positive effect when drawing probability curve afterward.

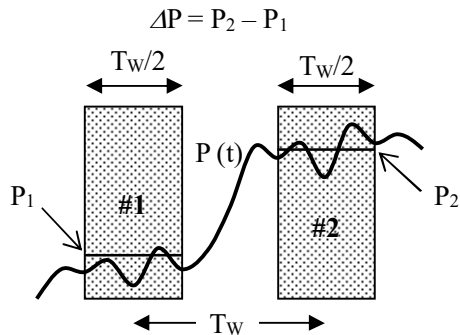


Fig. 1.22 Definition of ramp variation and T_w

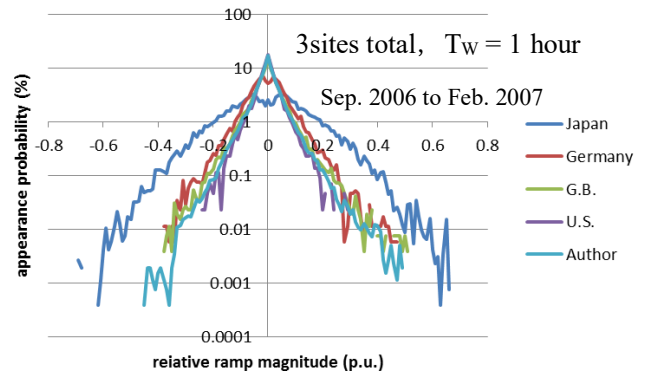


Fig. 1.23 Difference in probability curves by ramp definition

Ramp definitions by Germany, UK, US, Japan, and Author are applied to the same time sequential data, and probability curves are drawn as Fig. 1.23. The probability curves are called umbrella curve by their form. At one glance, only definition by Japan is different from the other four. Among them, definition by the author gives continuous and smooth probability curve toward very small probability. The merit contributes handling “rare but serious” ramp variation that is important for risk management. The merit derives from the second merit above, that reduction of data number is negligible small.

Difference of umbrella curves by T_w

Mutual smoothing effect (MSE) must operate also on ramp variation. MSE must be strong in slow large variation and is weak in fast small variation. Probability curves of three wind powers are calculated at ten-hour and one-hour T_w . The results are shown in Fig. 1.24.

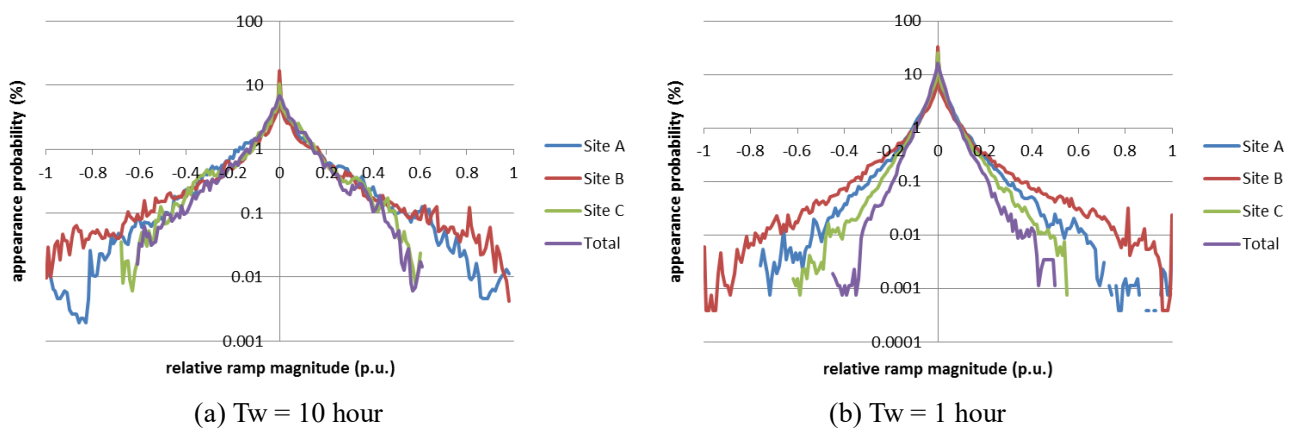


Fig. 1.24 Difference in umbrella curves by window span T_w

In case of 10 hour Tw, four curves of individual three and the total are almost piled up. This means MSE works poorly. On the contrary in case of 1 hour case, total probability curve is narrower than individual three site's probability curves. This means MSE works well.

2σ or 3σ ramp magnitude

As a method to quantitatively evaluate MSE on fast variation, the author presents 2σ or 3σ ramp variation. By drawing accumulated probability curve, variation magnitude over which larger variations do not appear in 2σ (95.44%) or 3σ (99.74%) probability can be calculated. Here, increase/decrease ramps are totally shown, but of course increase and decrease can be individually shown. 3σ accumulated probability curves of the three wind power at 1 hour Tw are drawn as Fig. 1.25.

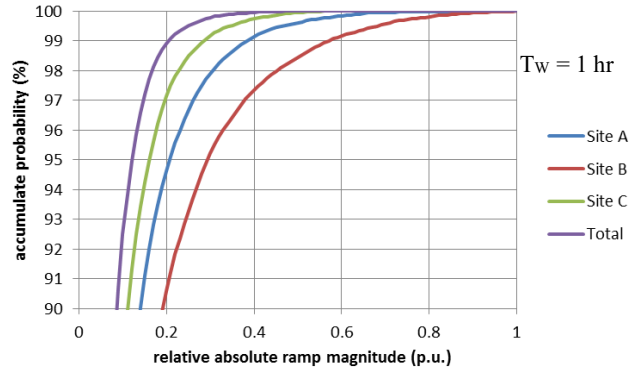


Fig. 1.25 3σ accumulated probability curves

This “2σ or 3σ ramp magnitude” varies by window span Tw. For every window span Tw, 2σ or 3σ ramp magnitudes of the three wind powers (A, B, C), total output (Mea), coherent hypothesis (Coh), and random hypothesis (Ran) are calculated as Fig. 1.26.

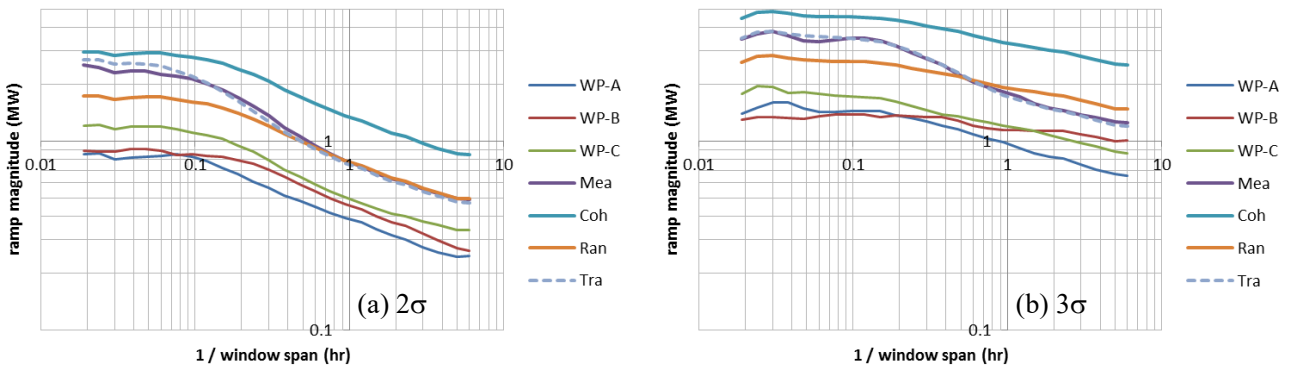


Fig. 1.26 2σ and 3σ ramp magnitude by window span Tw (Sep. 2006 to Feb. 2007)

Here applied transfer hypothesis. Since weak MSE is seen even in slow variation in wind power, a constant K is introduced as follows. Transfer swing period is expressed as Twx. Neq is equivalent number of WPs considering difference of their rated output.

$$\Delta P_{tra}(f) = K \Delta P_{coh}(f) \left| \frac{1 + j Twx f / \sqrt{Neq}}{1 + j Twx f} \right|$$

Parameters that makes accumulated square error between theoretical value (Tra) and measured value (ea) minimum are calculated as follows.

In case of 2σ: Twx = 8.74 hour, K = 0.921

In case of 3σ: Twx = 2.74 hour, K = 0.786

Transfer hypothesis agree with measured value (Mea) well.

Comparing 2σ case and 3σ case, T_{wx} is small in 3σ case, that is, MSE works poorly. Therefore, rare large variation is more serious in mutual smoothing than frequent medium sized variation.

Total ramp variation when 1000MW wind power penetrates in Hokuriku region is presumed using transfer hypothesis. 3σ ramp magnitude in which MSE works poorly is calculated as Fig. 1.27. Also measured ramp variation of demand is shown ($1/\pi$ in PV case is not adequate for wind power). In 1000MW penetration, wind power ramp variation is far smaller than demand variation.

However, additional study is needed. Calculation above presumed that wind power distributes evenly. In reality, wind power will concentrate in favorable region, and as the result, variation speed that MSE works well will shift to higher speed. In addition, ramp variation of demand is predicted very well, but wind power prediction is a developing technique. In these days, prediction error of tomorrow demand is around 2%. If prediction error of tomorrow wind power is around 10%, prediction error of wind power will exceed that of demand in ramp variation at 1 hour or longer time window. Thus, most serious research in near future is accurate prediction of ramp variation of wind power. That is already noticed generally, but the reason was not clear. The reason has become clear by study in this chapter.

References

- (1) Y. Yamagishi, T. Ueda, N. Kanao, and S. Komami: "A Study on the Wind Power Generation Fluctuation of Multiple Sites", IEEJ Trans. PE, Vol. 129 No. 6, pp.661-667 (2009)
- (2) H. Nagoya, S. Komami, and K. Ogimoto: "A Method for Presuming Total Output Fluctuation of Highly Penetrated Photovoltaic Generation Considering Mutual Smoothing Effect", IEEJ Trans. EIS, Vol.131, No. 10, pp.1688-1696 (2011)
- (3) S. Komami and T. Jozuka: "Factors That Affect Transfer Swing Period in Mutual Smoothing Effect of RE Output Fluctuation", being submitted to IEEJ Trans. PE (2017)
- (4) Y. Yamagishi, H. Nagoya, S. Komami, and K. Ogimoto: "Estimation of Photovoltaic Generation Output Fluctuation Considering Reduction of Smoothing Effect by Uneven Distribution", IEEJ trans. EIS, Vol. 131, No. 10, pp.1722-1729 (2011)
- (5) H. Nagoya, S. Komami, and K. Ogimoto: "A Study on Analysis of Presumed Highly Penetrated PV's Total Output", IEEJ 2012 Annual Conference No. 6-010 (2012)
- (6) H. Nagoya, S. Komami, and K. ogimoto: "A Methodfor Load Frequency Control Using Battery in Power System with Highly Penetrated Photovoltaic Generation", IEEJ Trans. PE, Vol. 132, No. 4, pp.325-333 (2012)

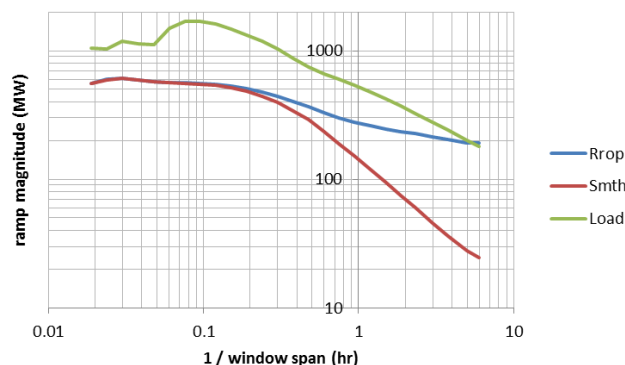


Fig 1.27 3σ ramp magnitude of 1000MW wind power